Electronic Supplementary Material (ESI) for Polymer Chemistry.

Electronic Supplementary Information

for

Controlled and Effective Ring-Opening (Co)Polymerization of *rac*-Lactide, ε-Caprolactone and ε-Decalactone by β-Pyrimidyl Enolate Aluminum Complexes

Sirawan Kamavichanurat, Kunanon Jampakaew and Pimpa Hormnirun[*]

[a]Laboratory of Catalysts and Advanced Polymer Materials, Department of Chemistry and Center of Excellence for Innovation in Chemistry, Faculty of Science, Kasetsart University, Bangkok 10900, Thailand

[b]Center for Advanced Studies in Nanotechnology for Chemical, Food and Agricultural Industries, Kasetsart University, Bangkok 10900, Thailand.

*E-mail: fscipph@ku.ac.th

Content

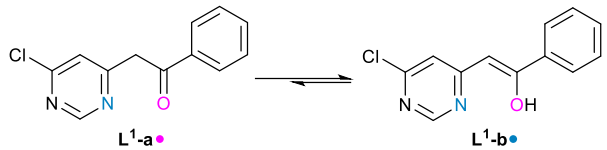

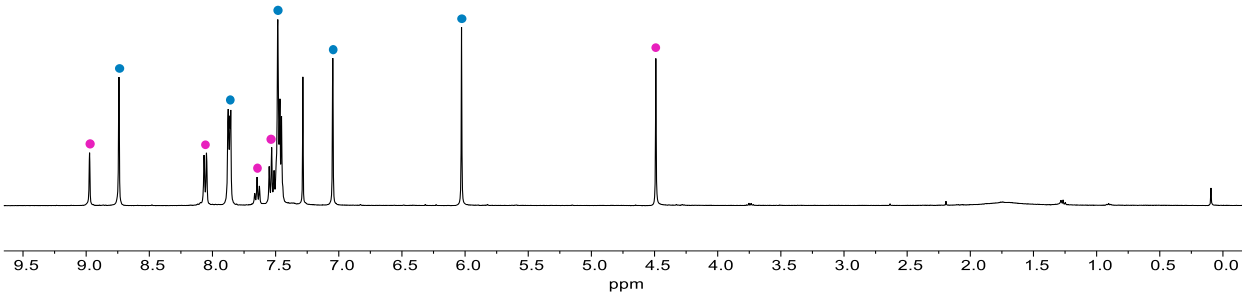

Fig. S1 ^{1}H NMR spectrum of **L^{1}** in $CDCl_3$ at 298 K.

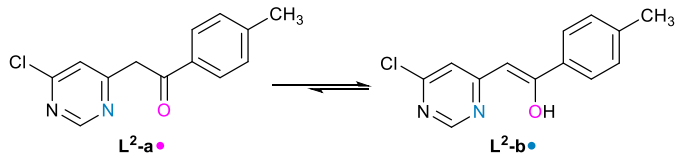

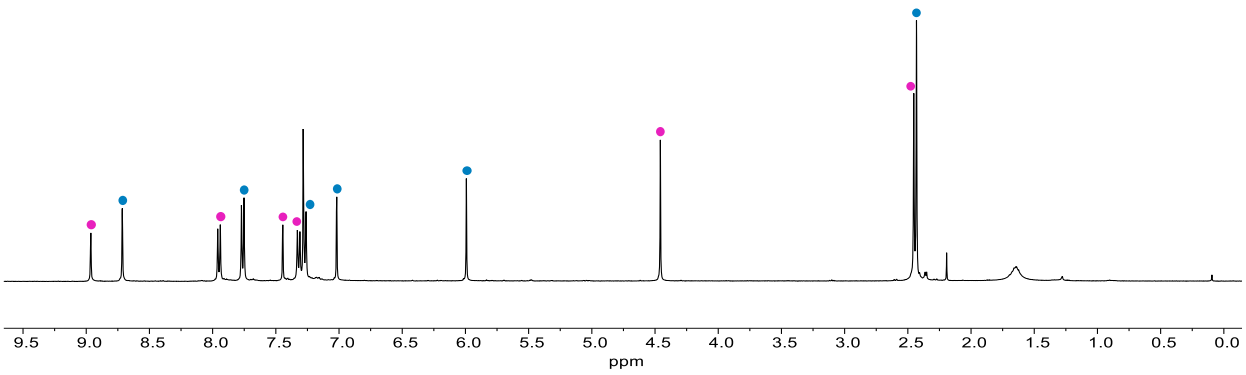

Fig. S2 ^{1}H NMR spectrum of **L^{2}** in $CDCl_3$ at 298 K.

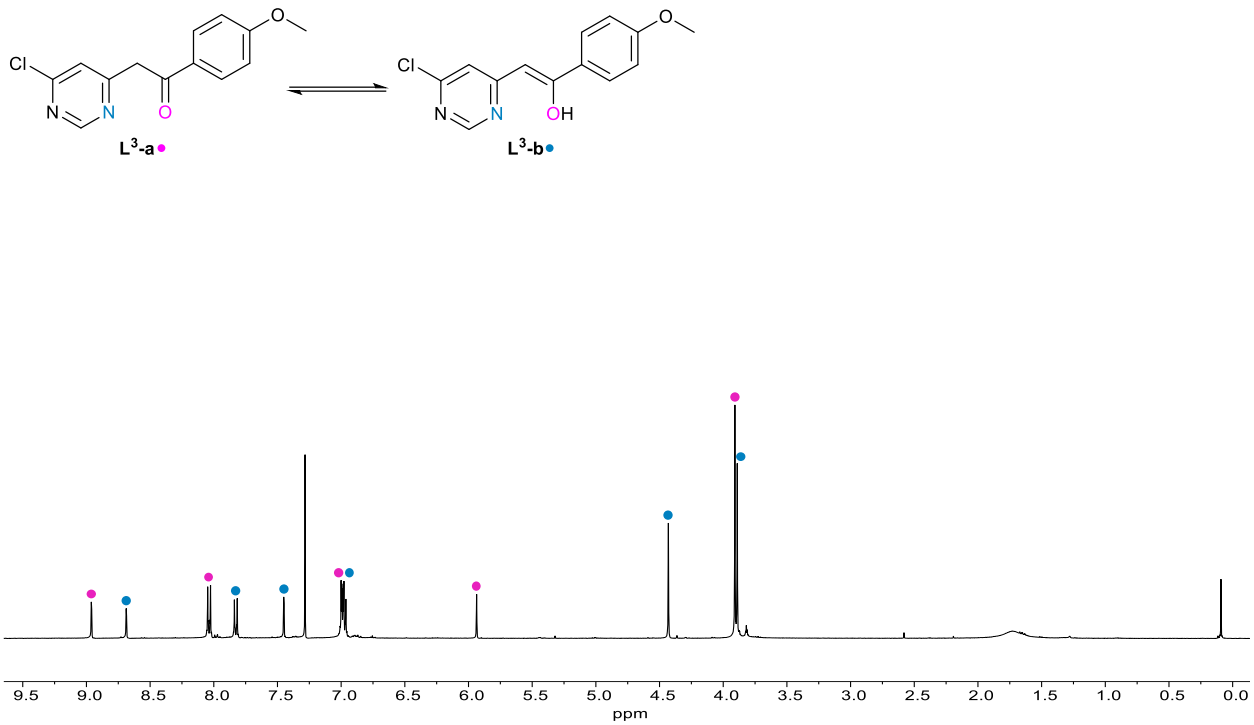

Fig. S3 ^{1}H NMR spectrum of **L^{3}** in $CDCl_3$ at 298 K.

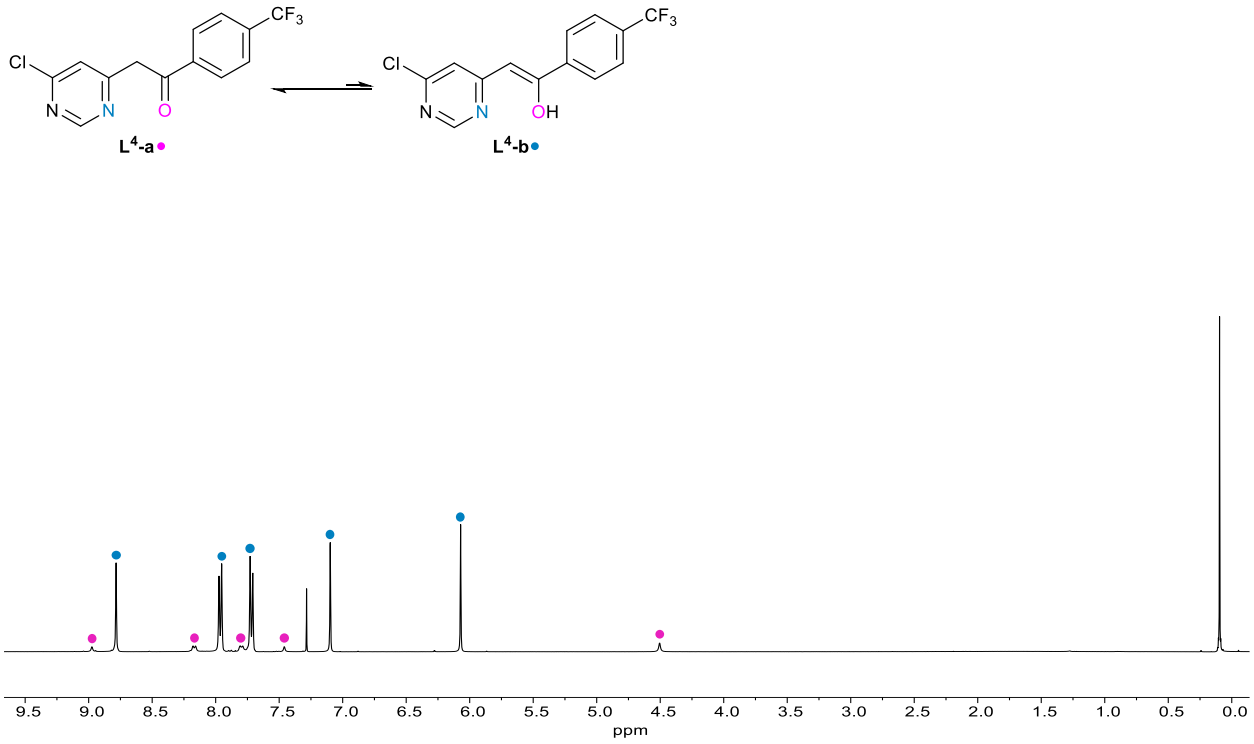

Fig. S4 ^{1}H NMR spectrum of **L^{4}** in $CDCl_3$ at 298 K.

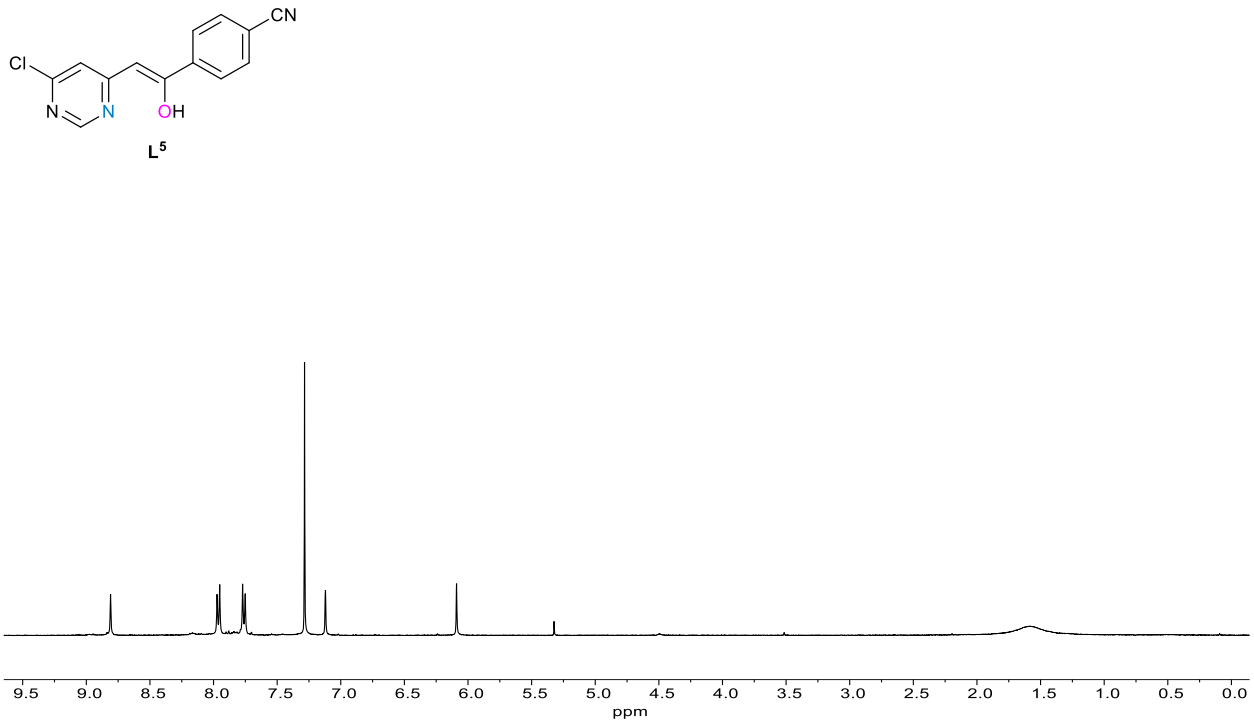

Fig. S5 ^{1}H NMR spectrum of **L^{5}** in $CDCl_3$ at 298 K.

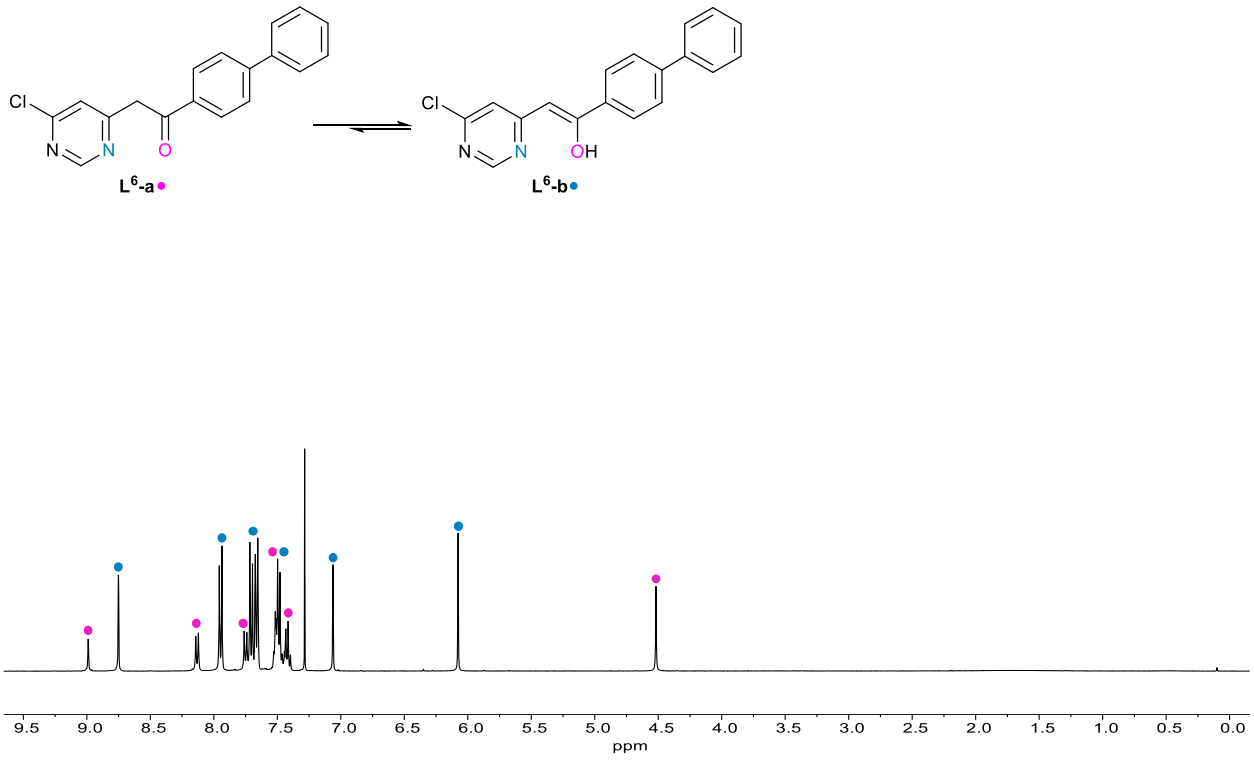

Fig. S6 ^{1}H NMR spectrum of **L^{6}** in $CDCl_3$ at 298 K.

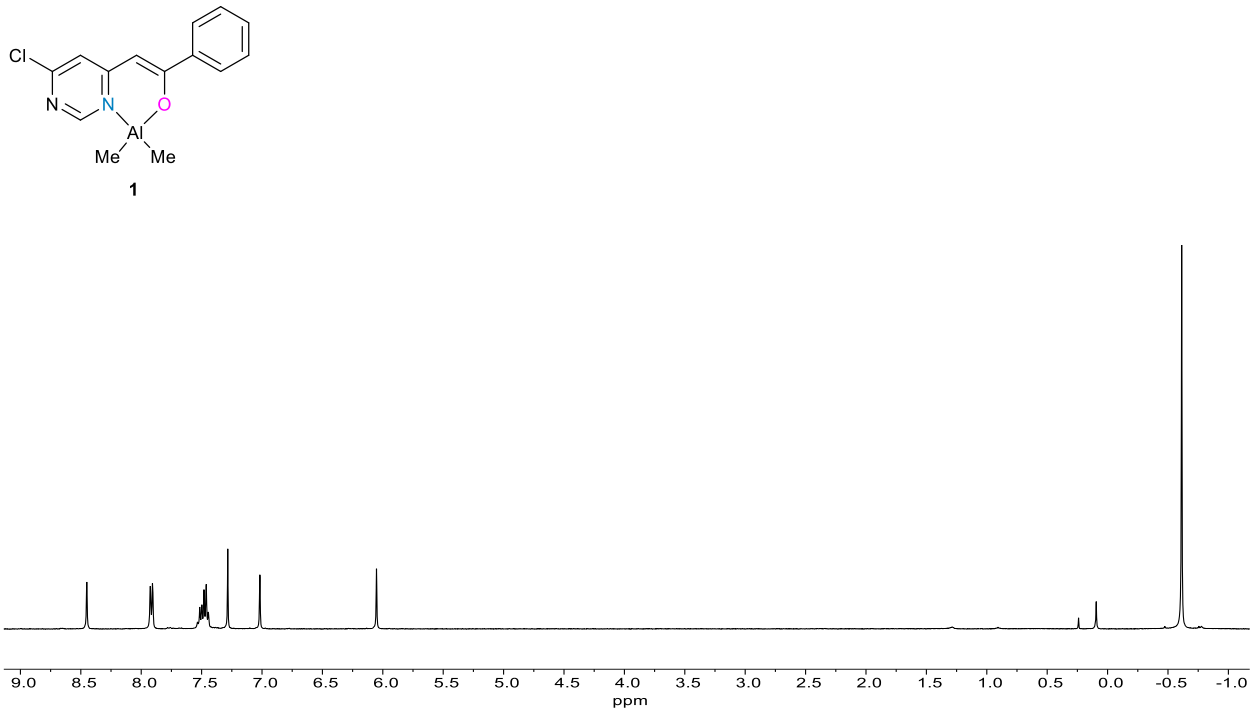

Fig. S7 ^{1}H NMR spectrum of **1** in $CDCl_3$ at 298 K.

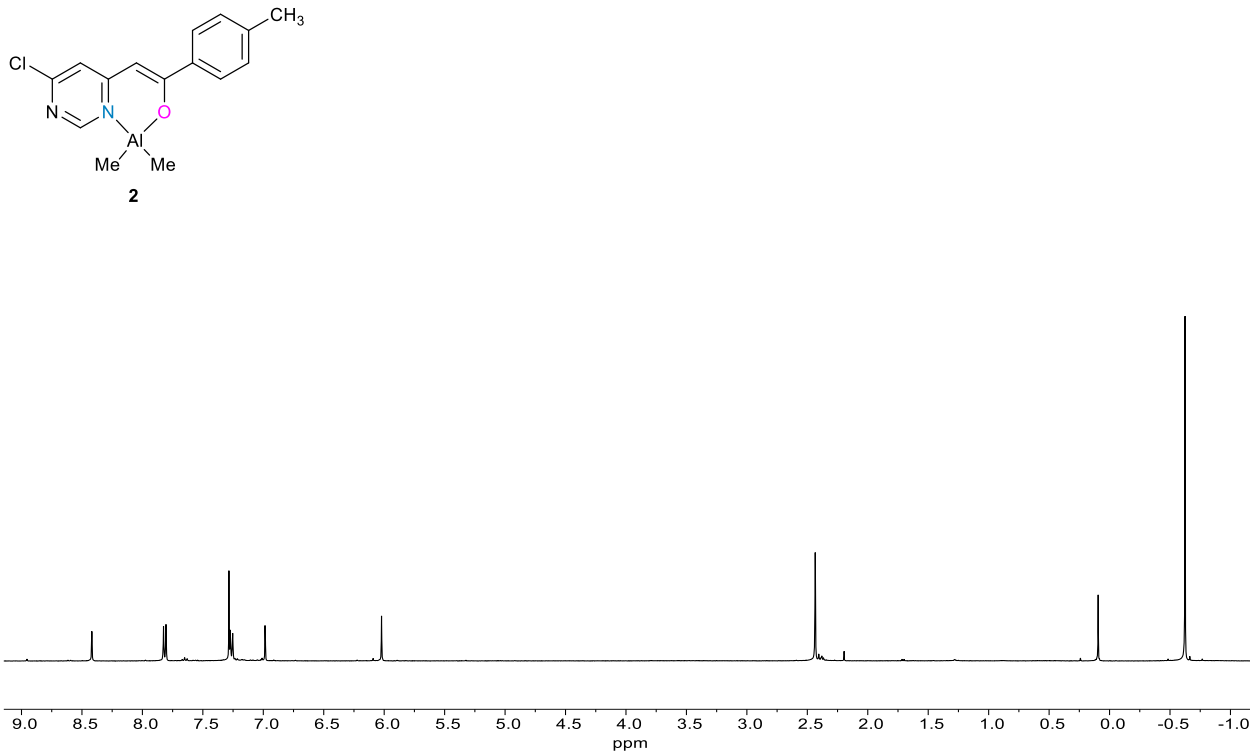

Fig. S8 ^{1}H NMR spectrum of **2** in $CDCl_3$ at 298 K.

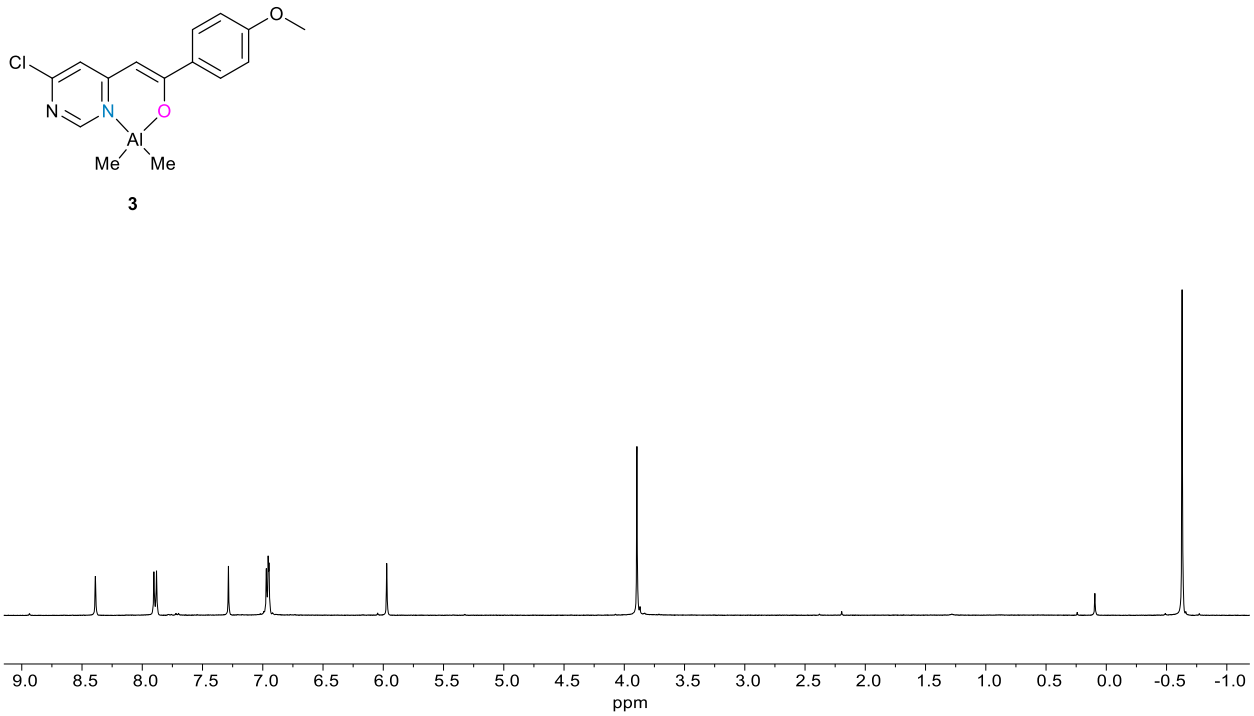

Fig. S9 ^{1}H NMR spectrum of **3** in $CDCl_3$ at 298 K.

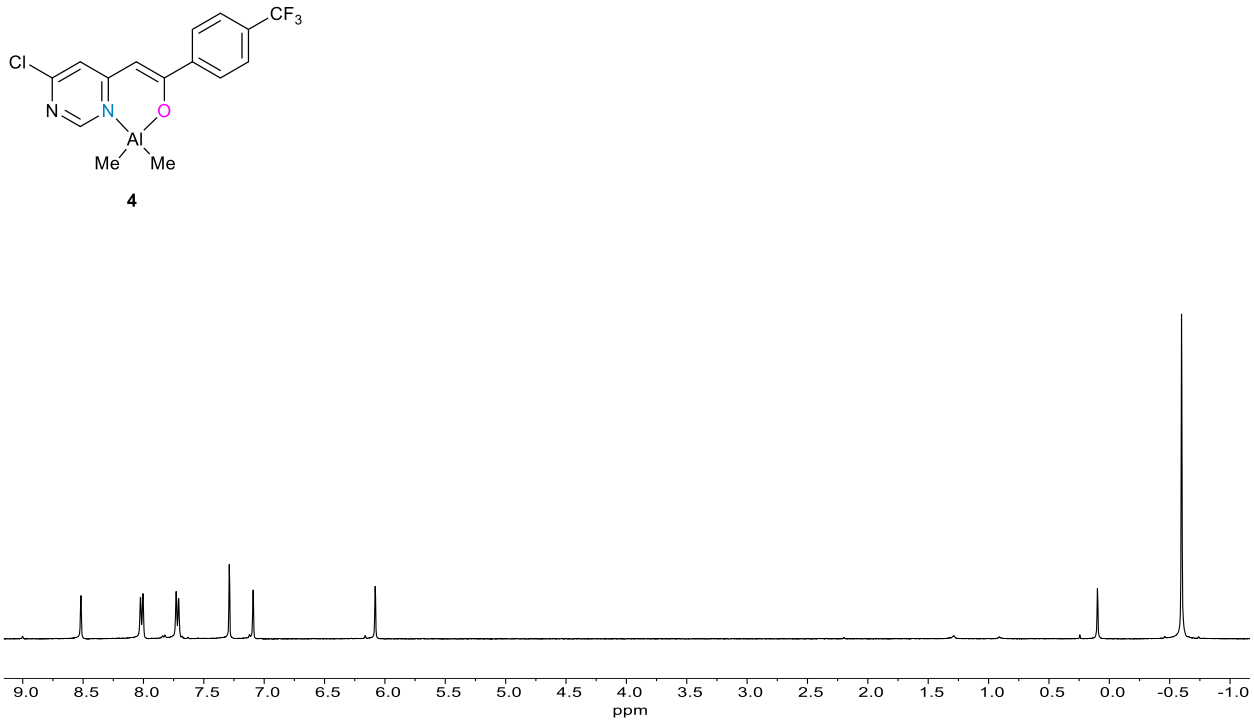

Fig. S10 ^{1}H NMR spectrum of **4** in $CDCl_3$ at 298 K.

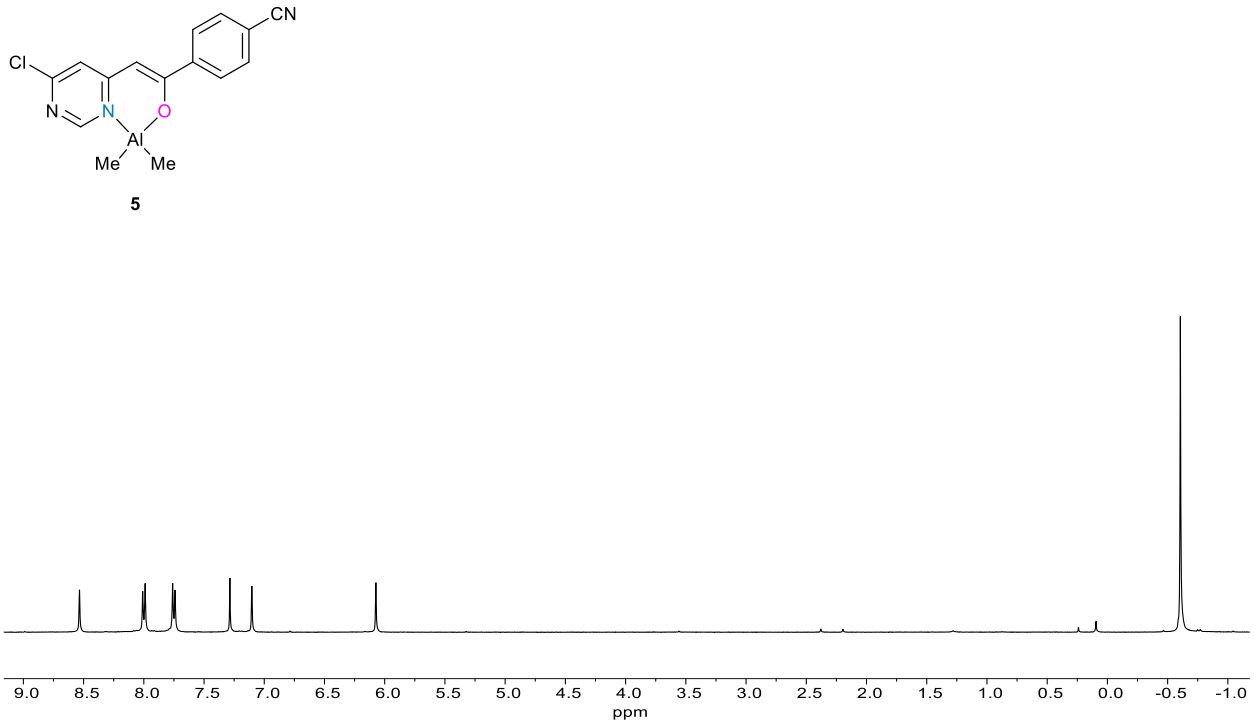

Fig. S11 ^{1}H NMR spectrum of **5** in $CDCl_3$ at 298 K.

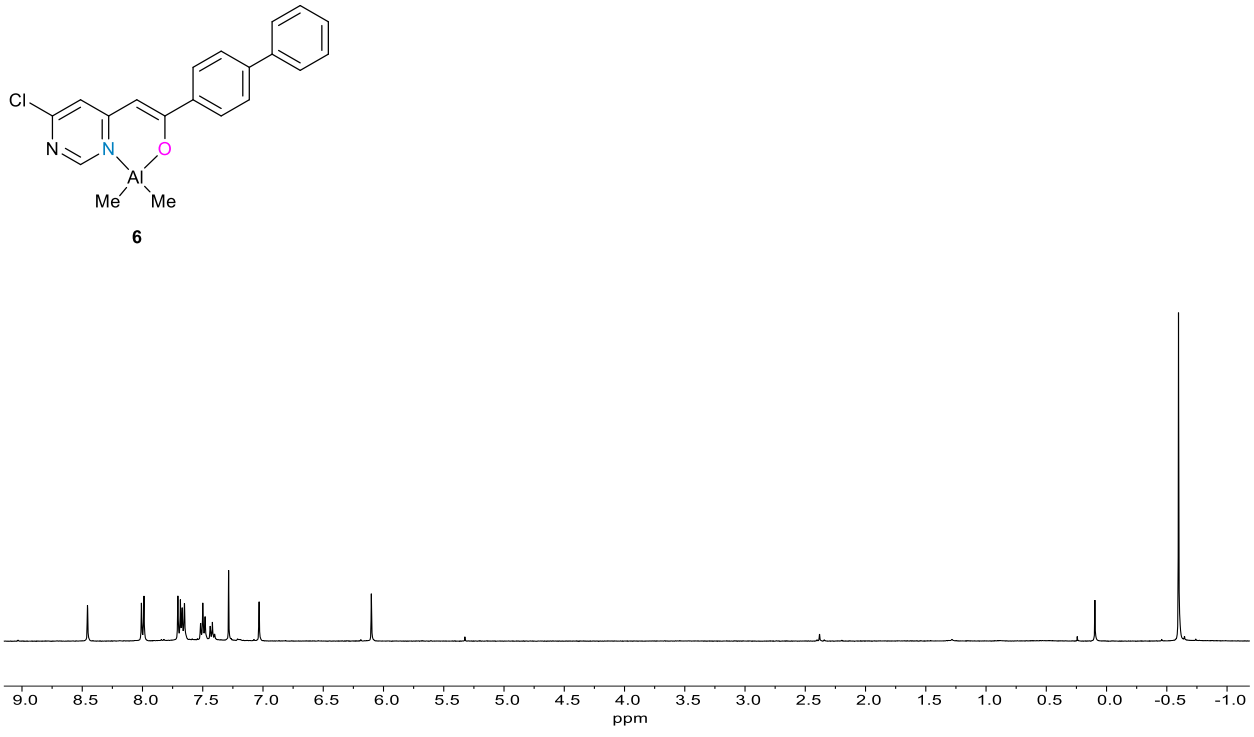

Fig. S12 ^{1}H NMR spectrum of **6** in $CDCl_3$ at 298 K.

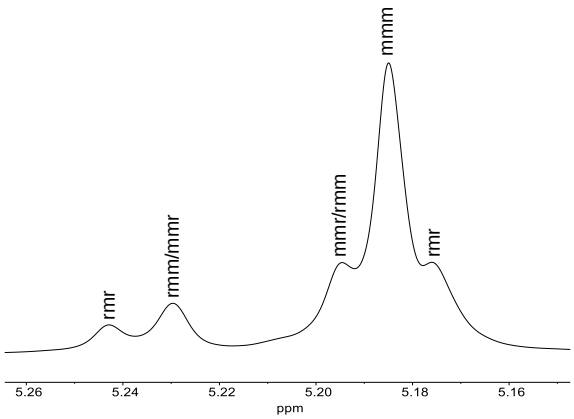

Fig. S13 Homonuclear decoupled ^{1}H NMR spectrum of the methine region of PLA prepared from *rac*-LA at 70 ºC in toluene (400 MHz, $CDCl_3$) with complex **1**.

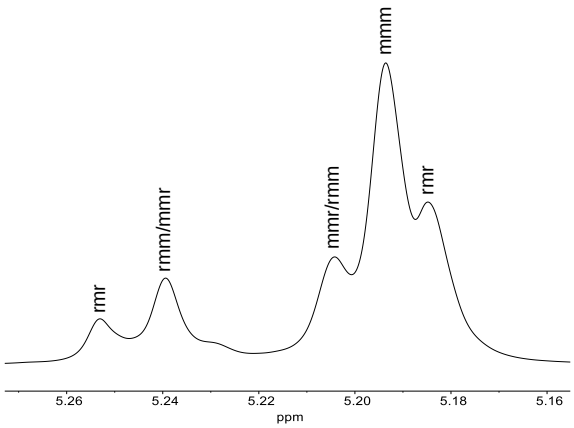

Fig. S14 Homonuclear decoupled ^{1}H NMR spectrum of the methine region of PLA prepared from *rac*-LA at 70 ºC in toluene (400 MHz, $CDCl_3$) with complex **2**.

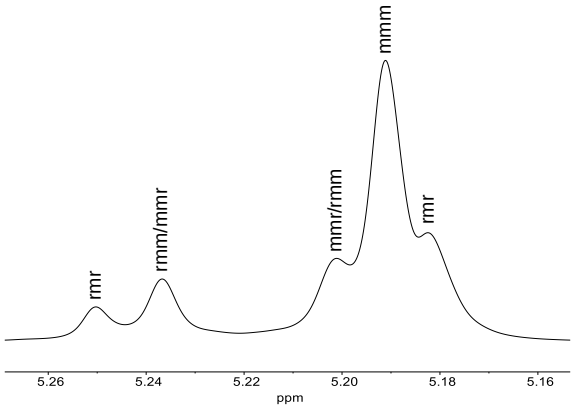

Fig. S15 Homonuclear decoupled ^{1}H NMR spectrum of the methine region of PLA prepared from *rac*-LA at 70 ºC in toluene (400 MHz, $CDCl_3$) with complex **3**.

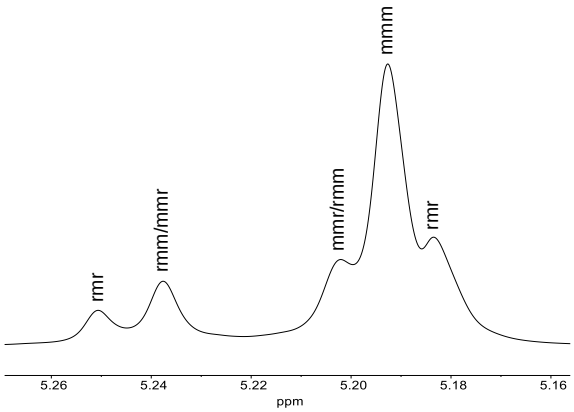

Fig. S16 Homonuclear decoupled ^{1}H NMR spectrum of the methine region of PLA prepared from *rac*-LA at 70 ºC in toluene (400 MHz, $CDCl_3$) with complex **4**.

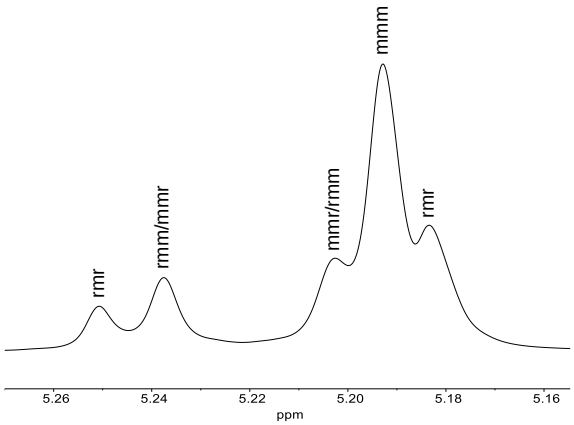

Fig. S17 Homonuclear decoupled ^{1}H NMR spectrum of the methine region of PLA prepared from *rac*-LA at 70 ºC in toluene (400 MHz, $CDCl_3$) with complex **5**.

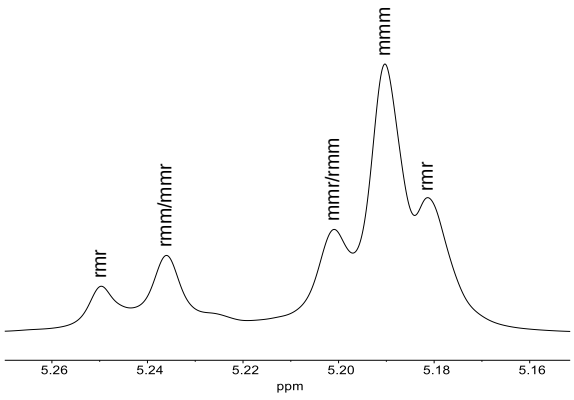

Fig. S18 Homonuclear decoupled ^{1}H NMR spectrum of the methine region of PLA prepared from *rac*-LA at 70 ºC in toluene (400 MHz, $CDCl_3$) with complex **6**.

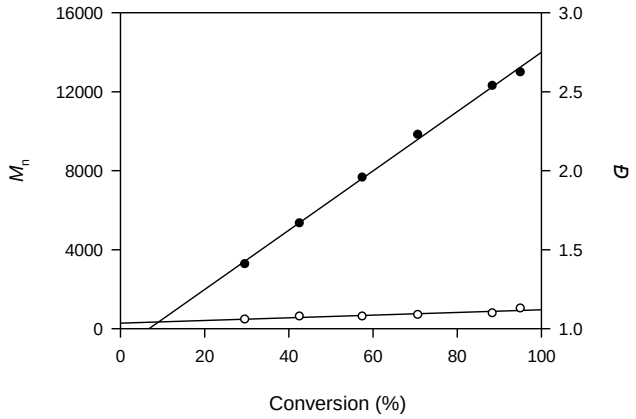

Fig. S19 Plot of the PCL M_n (●) (versus polystyrene standards) and $Đ$ (○) as a function of monomer conversion for PCL using BnOH as an initiator ($[CL]_0/[Al]$ = 100, toluene, 70 °C).

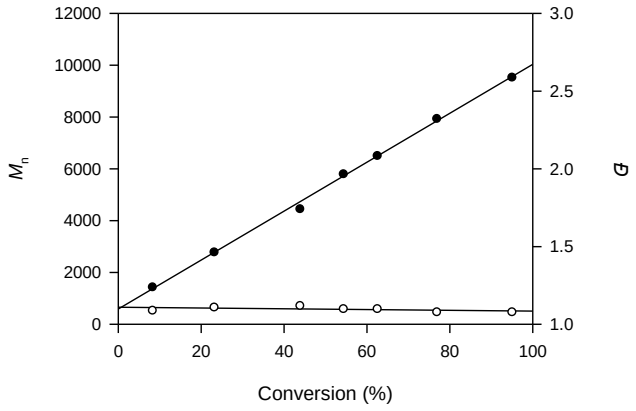

Fig. S20 Plot of the PDL M_n (●) (versus polystyrene standards) and $Đ$ (○) as a function of monomer conversion for PDL using BnOH as an initiator ($[DL]_0/[Al]$ = 50, toluene, 70 °C).

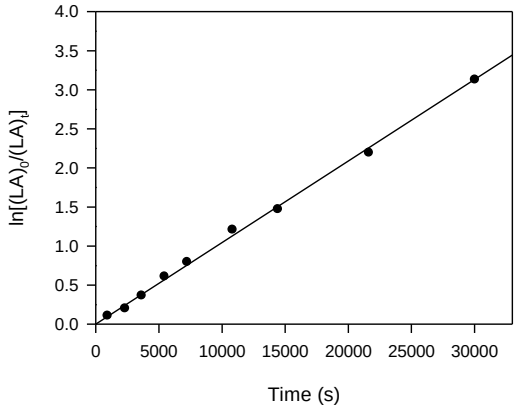

Fig. S21 Semilogarithmic plot of *rac*-LA conversion versus time in toluene at 70 °C with complex **1** ($[LA]_0/[Al]$ = 50:1, $[LA]_0$ = 0.42 M, [Al] = 8.33 mM).

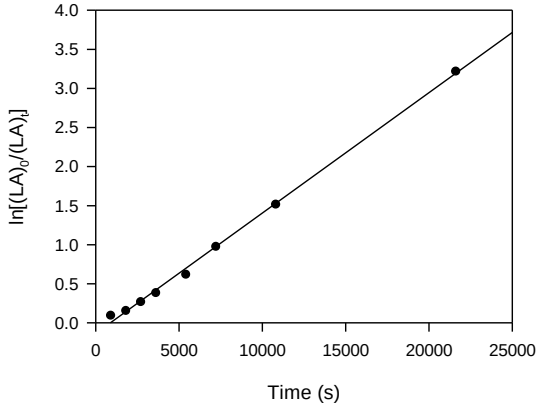

Fig. S22 Semilogarithmic plot of *rac*-LA conversion versus time in toluene at 70 °C with complex **2** ($[LA]_0/[Al]$ = 50:1, $[LA]_0$ = 0.42 M, [Al] = 8.33 mM).

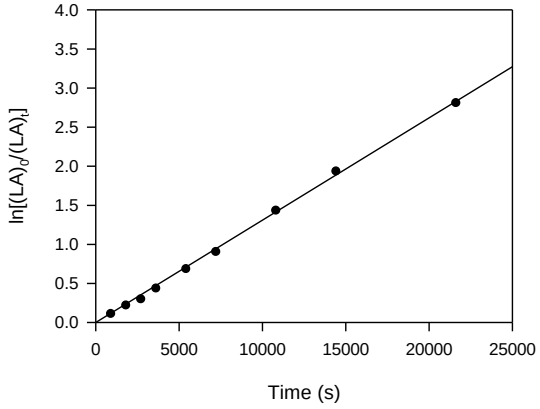

Fig. S23 Semilogarithmic plot of *rac*-LA conversion versus time in toluene at 70 °C with complex **3** ($[LA]_0/[Al]$ = 50:1, $[LA]_0$ = 0.42 M, [Al] = 8.33 mM).

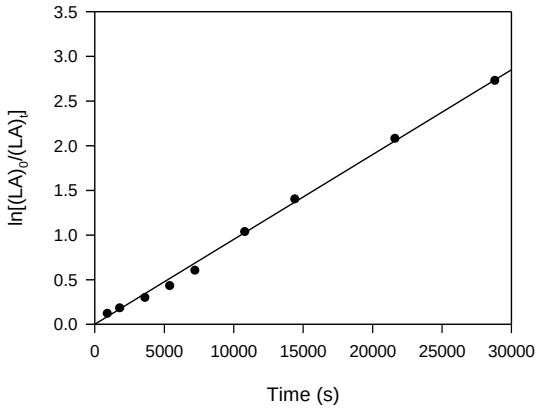

Fig. S24 Semilogarithmic plot of *rac*-LA conversion versus time in toluene at 70 °C with complex **5** ($[LA]_0/[Al]$ = 50:1, $[LA]_0$ = 0.42 M, [Al] = 8.33 mM).

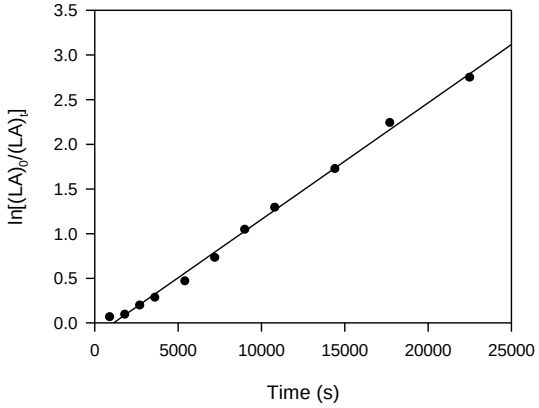

Fig. S25 Semilogarithmic plot of *rac*-LA conversion versus time in toluene at 70 °C with complex **6** ($[LA]_0/[Al]$ = 50:1, $[LA]_0$ = 0.42 M, [Al] = 8.33 mM).

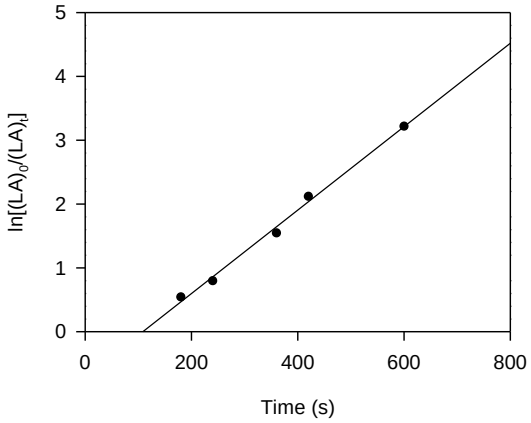

Fig. S26 Semilogarithmic plot of ε-CL conversion versus time in toluene at 70 °C with complex **1** ($[CL]_0/[Al]$=100:1, $[CL]_0$ = 1.25 M, [Al] = 12.50 mM).

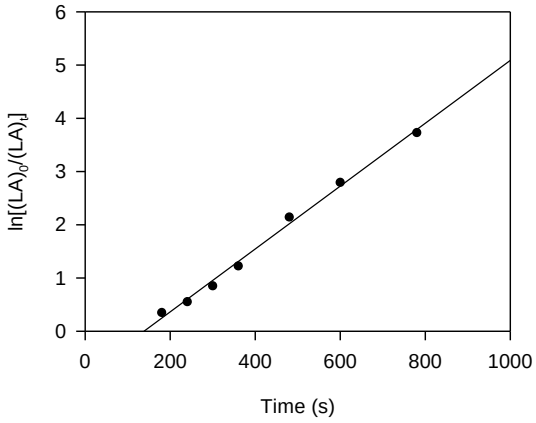

Fig. S27 Semilogarithmic plot of ε-CL conversion versus time in toluene at 70 °C with complex **2** ($[CL]_0/[Al]=100:1$, $[CL]_0 = 1.25$ M, [Al] = 12.50 mM).

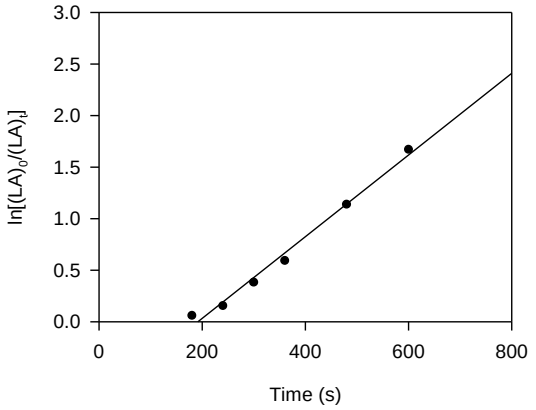

Fig. S28 Semilogarithmic plot of ε-CL conversion versus time in toluene at 70 °C with complex **3** ($[CL]_0/[Al]=100:1$, $[CL]_0 = 1.25$ M, [Al] = 12.50 mM).

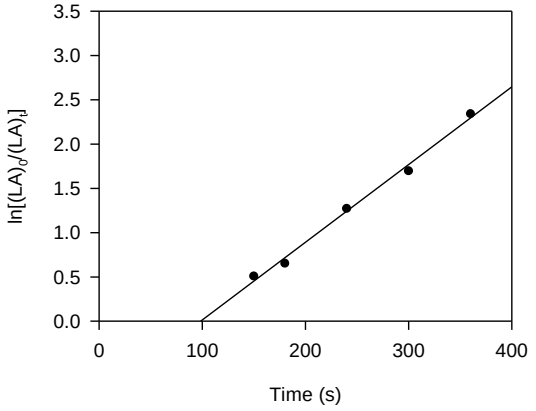

Fig. S29 Semilogarithmic plot of ε-CL conversion versus time in toluene at 70 °C with complex **4** ($[CL]_0/[Al]=100:1$, $[CL]_0 = 1.25$ M, [Al] = 12.50 mM).

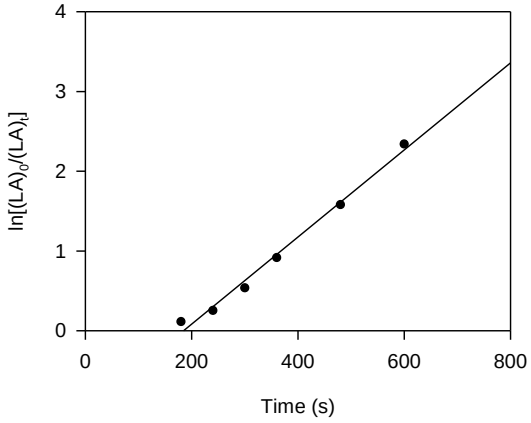

Fig. S30 Semilogarithmic plot of ε-CL conversion versus time in toluene at 70 °C with complex **5** ($[CL]_0/[Al]$=100:1, $[CL]_0$ = 1.25 M, [Al] = 12.50 mM).

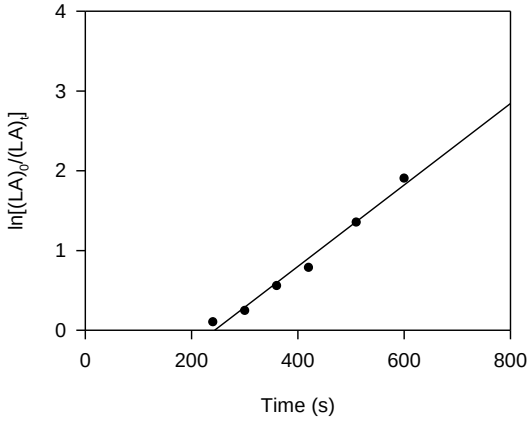

Fig. S31 Semilogarithmic plot of ε-CL conversion versus time in toluene at 70 °C with complex **6** ($[CL]_0/[Al]$=100:1, $[CL]_0$ = 1.25 M, [Al] = 12.50 mM).

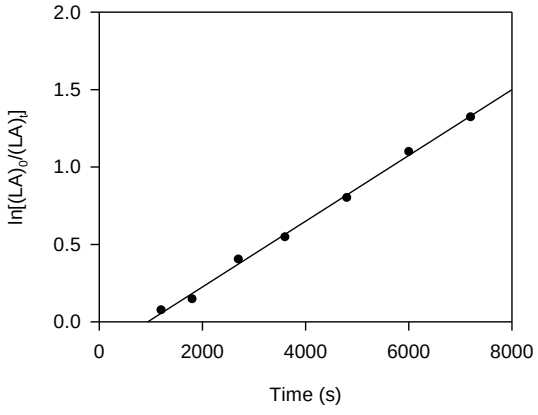

Fig. S32 Semilogarithmic plot of ε-DL conversion versus time in toluene at 70 °C with complex **1** ($[DL]_0/[Al]$=50:1, $[DL]_0$ = 0.62 M, [Al] = 12.50 mM).

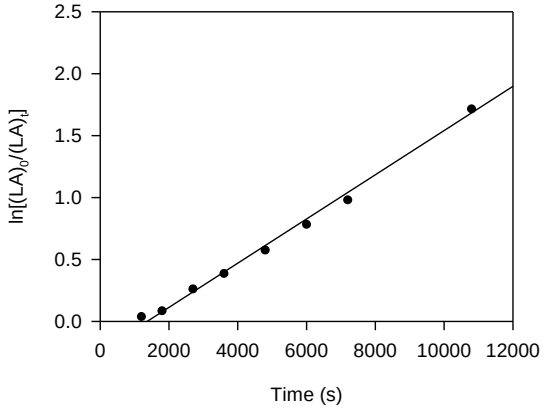

Fig. S33 Semilogarithmic plot of ε-DL conversion versus time in toluene at 70 °C with complex **2** ($[DL]_0/[Al]$=50:1, $[DL]_0$ = 0.62 M, [Al] = 12.50 mM).

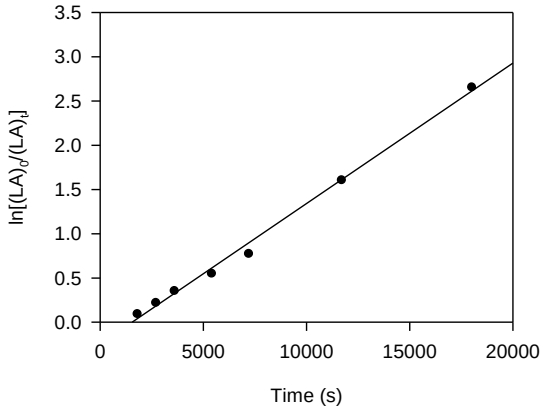

Fig. S34 Semilogarithmic plot of ε-DL conversion versus time in toluene at 70 °C with complex **3** ($[DL]_0/[Al]$=50:1, $[DL]_0$ = 0.62 M, [Al] = 12.50 mM).

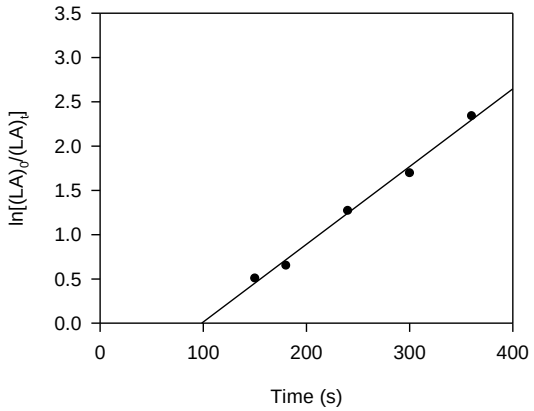

Fig. S35 Semilogarithmic plot of ε-DL conversion versus time in toluene at 70 °C with complex **4** ($[DL]_0/[Al]$=50:1, $[DL]_0$ = 0.62 M, [Al] = 12.50 mM).

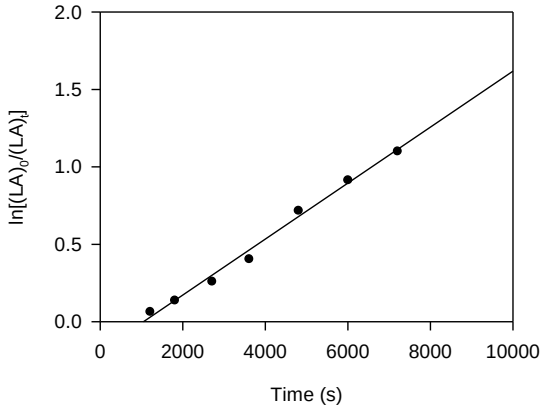

Fig. S36 Semilogarithmic plot of ε-DL conversion versus time in toluene at 70 °C with complex **5** ($[DL]_0/[Al]$=50:1, $[DL]_0$ = 0.62 M, [Al] = 12.50 mM).

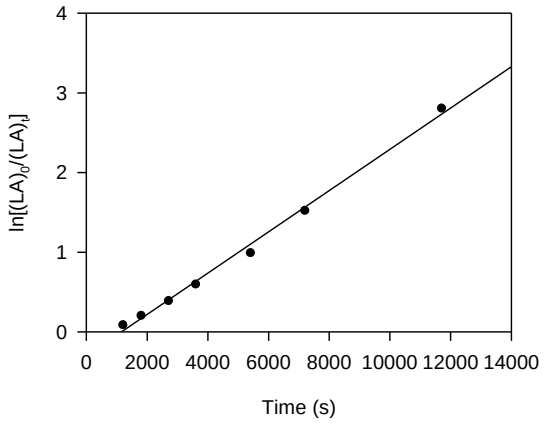

Fig. S37 Semilogarithmic plot of ε-DL conversion versus time in toluene at 70 °C with complex **6** ($[DL]_0/[Al]$=50:1, $[DL]_0$ = 0.62 M, [Al] = 12.50 mM).

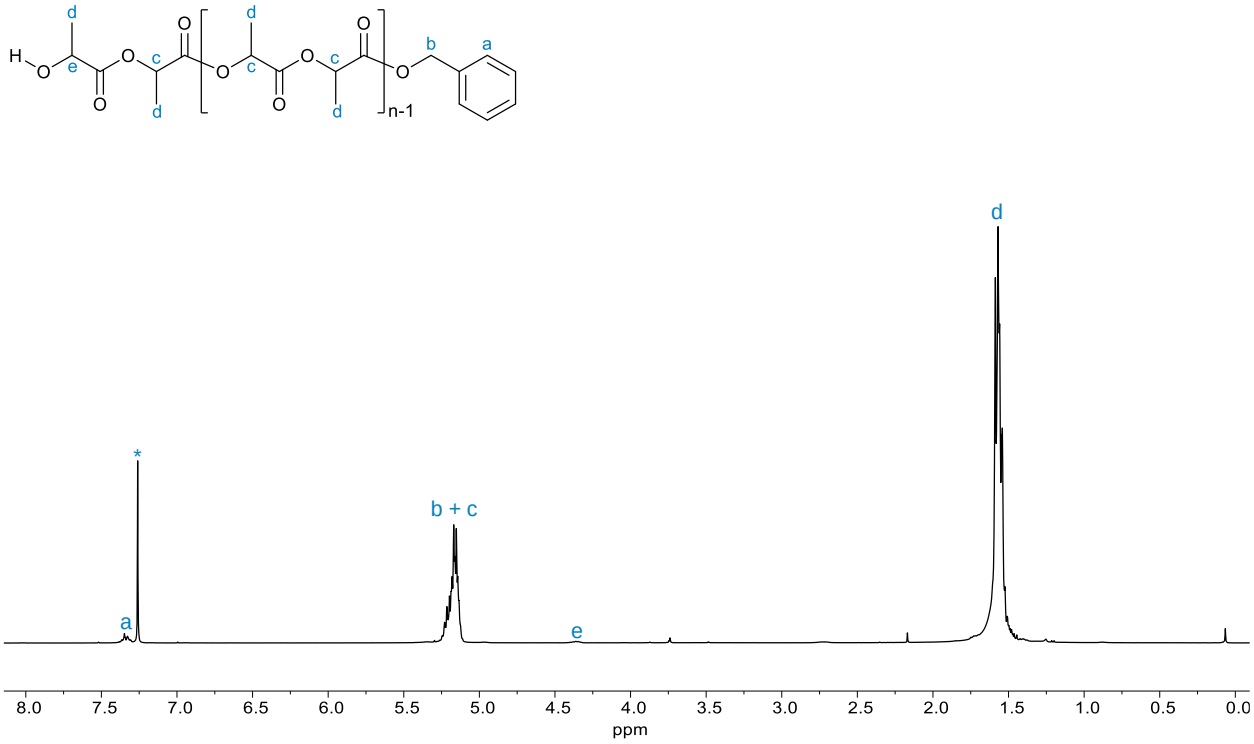

Fig. S38 ^{1}H NMR spectrum of PLA initiated by **3** in $CDCl_3$ at 298 K (* = solvent residue peak).

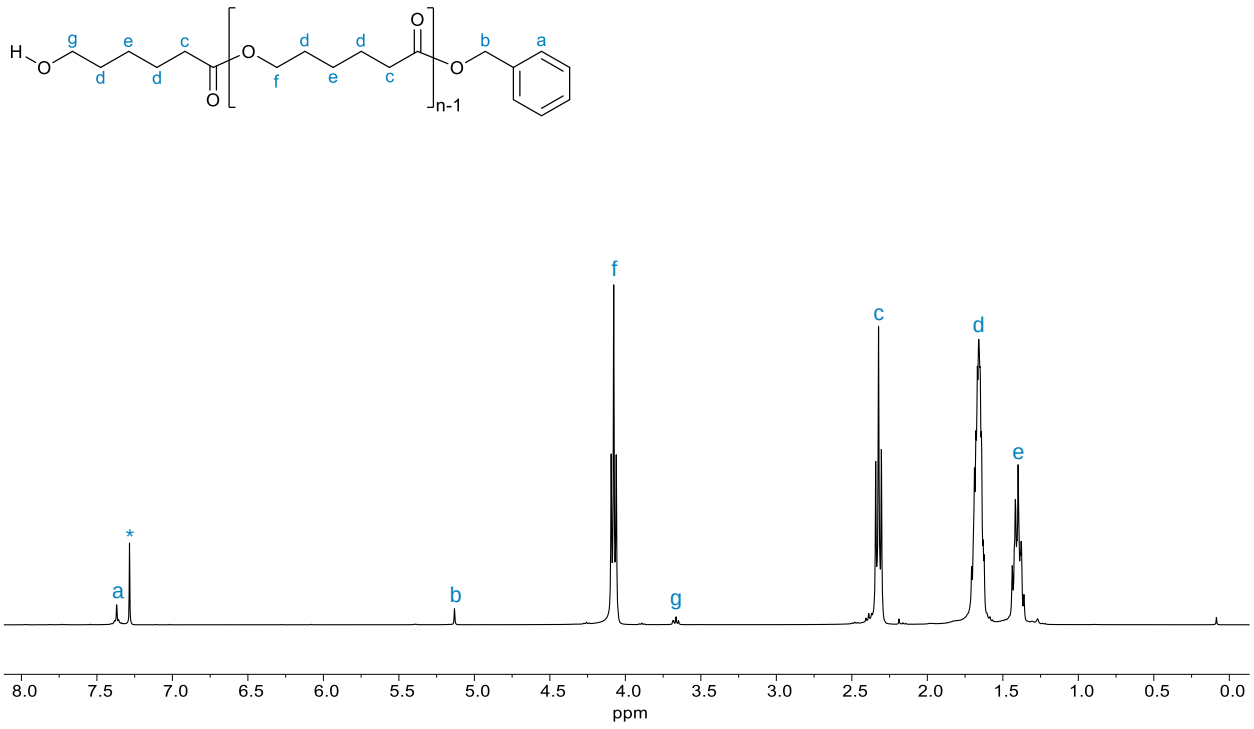

Fig. S39 ^{1}H NMR spectrum of PCL initiated by **4** in $CDCl_3$ at 298 K (* = solvent residue peak).

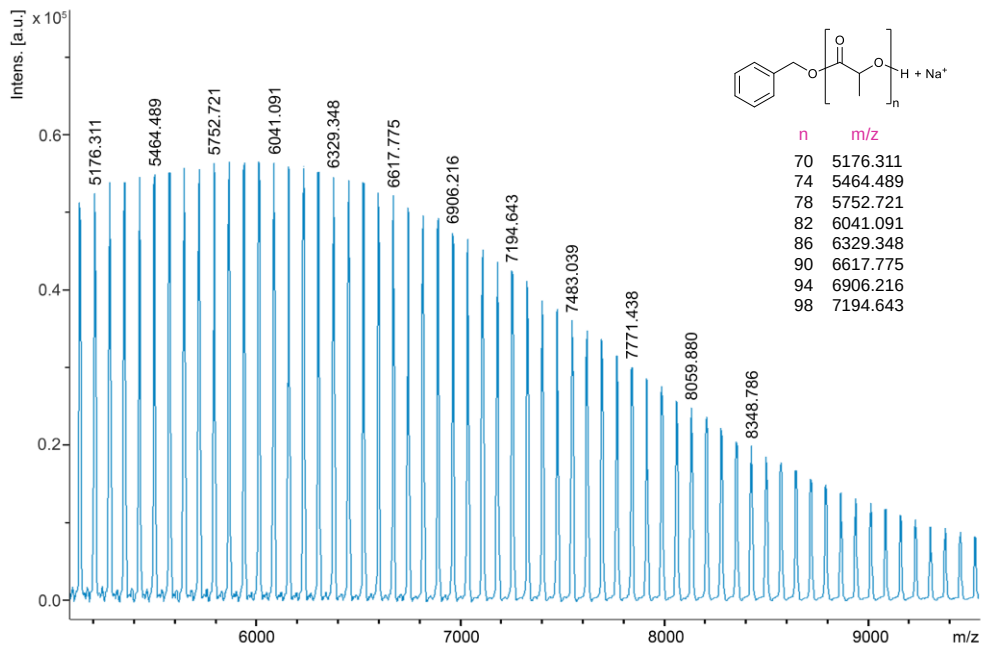

$C_6H_5CH_2O–[C(O)CH(CH_2)O]_n–H + Na$ (n =78)
The calculated theoretical value = 108.06 + 78(72.02) + 22.99 = 5748.61.

Fig. S40 MALDI-TOF mass spectrum of PLA initiated by **3** in toluene at 70 °C.

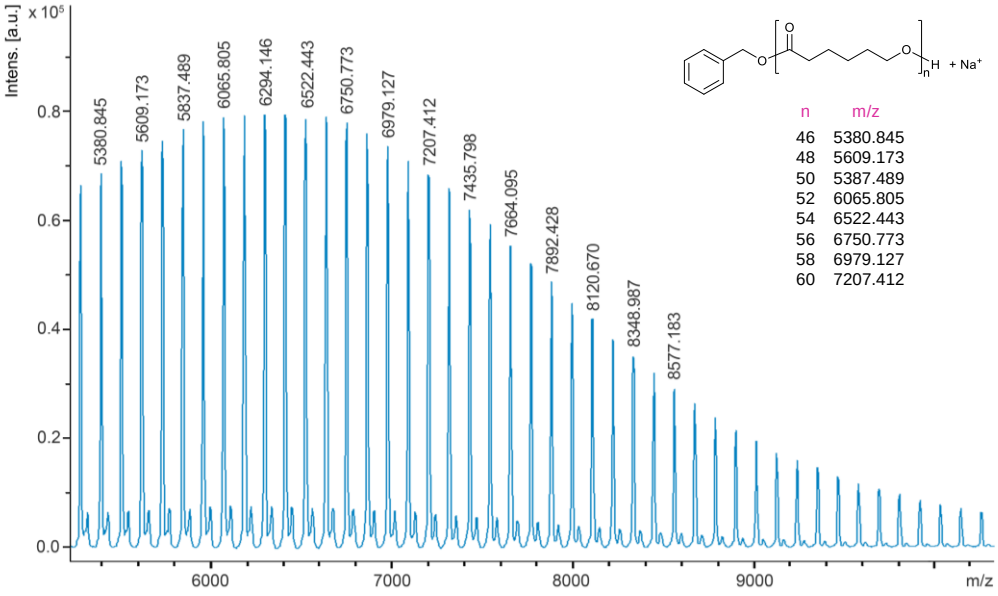

$C_6H_5CH_2O–[C(O)(CH_2)_5O]_n–H + Na$ (n =48)
The calculated theoretical value = 108.06 + 48(114.07) + 22.99 = 5606.41.

Fig. S41 MALDI-TOF mass spectrum of PCL initiated by **4** in toluene at 70 °C.

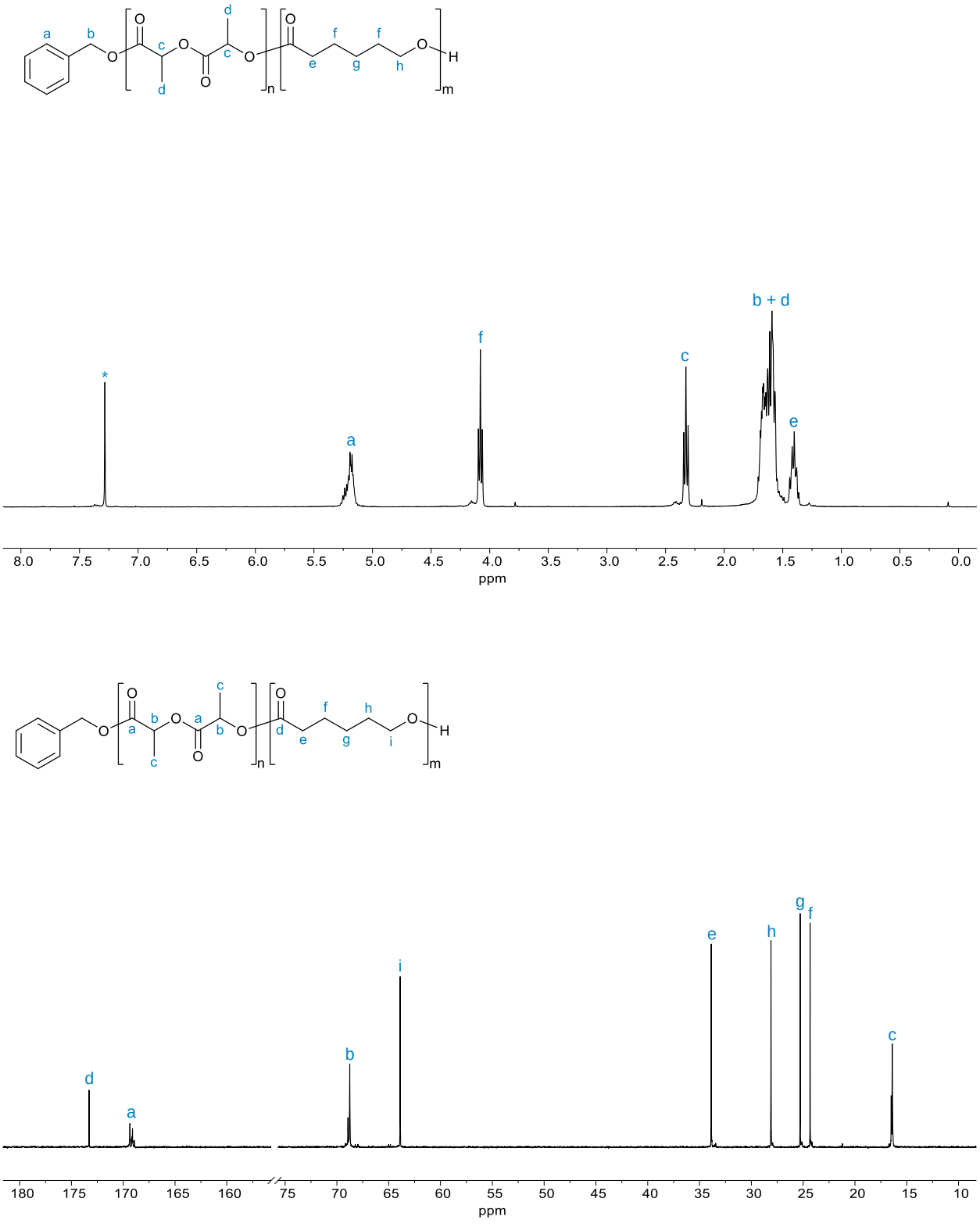

Fig. S42 ^{1}H and $^{13}C\{H\}$ NMR spectrum of poly(*rac*-LA-*b*-CL) in $CDCl_3$ at 298 K.

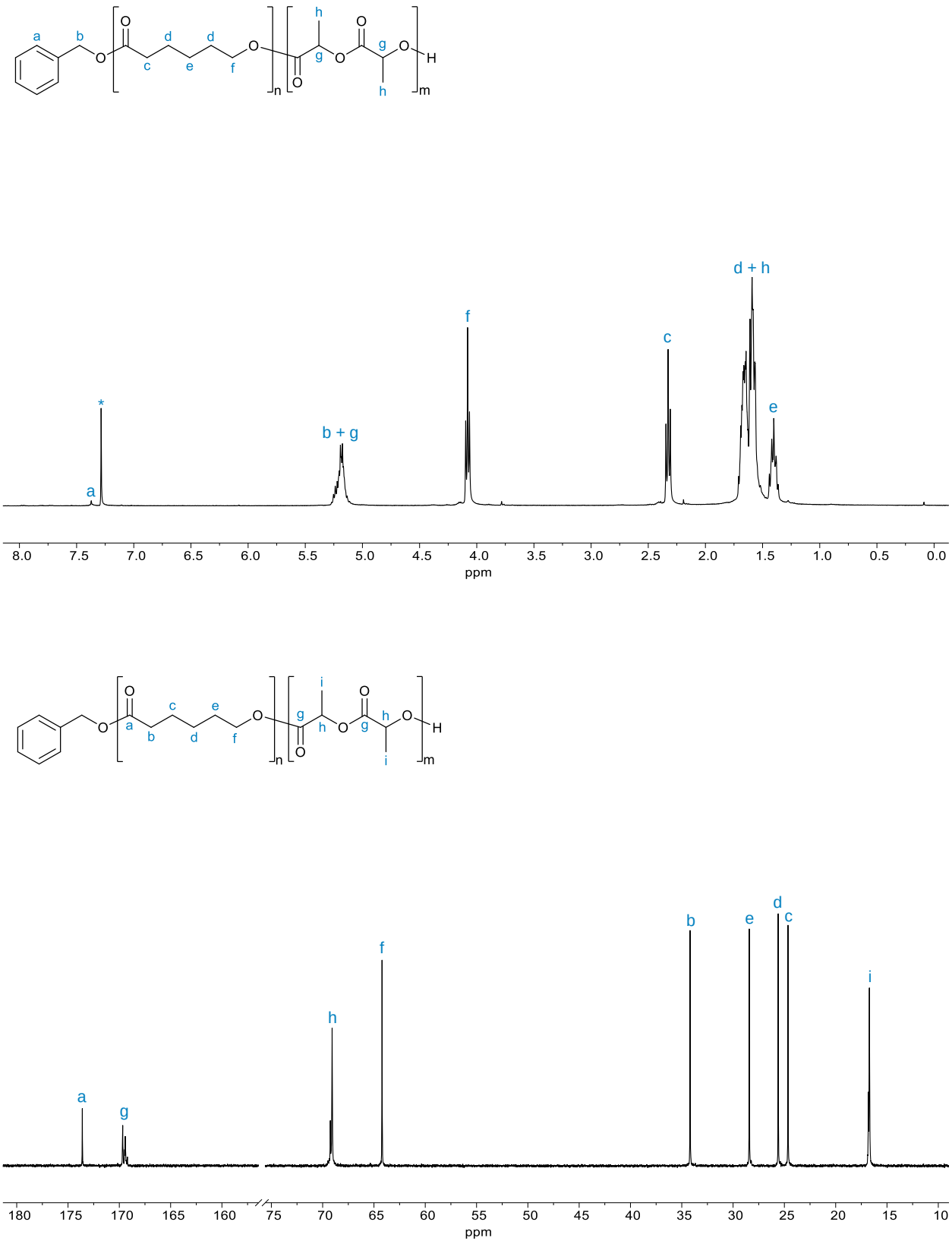

Fig. S43 ^{1}H and $^{13}C\{H\}$ NMR spectrum of poly(CL-*b*- *rac*-LA) in $CDCl_3$ at 298 K.

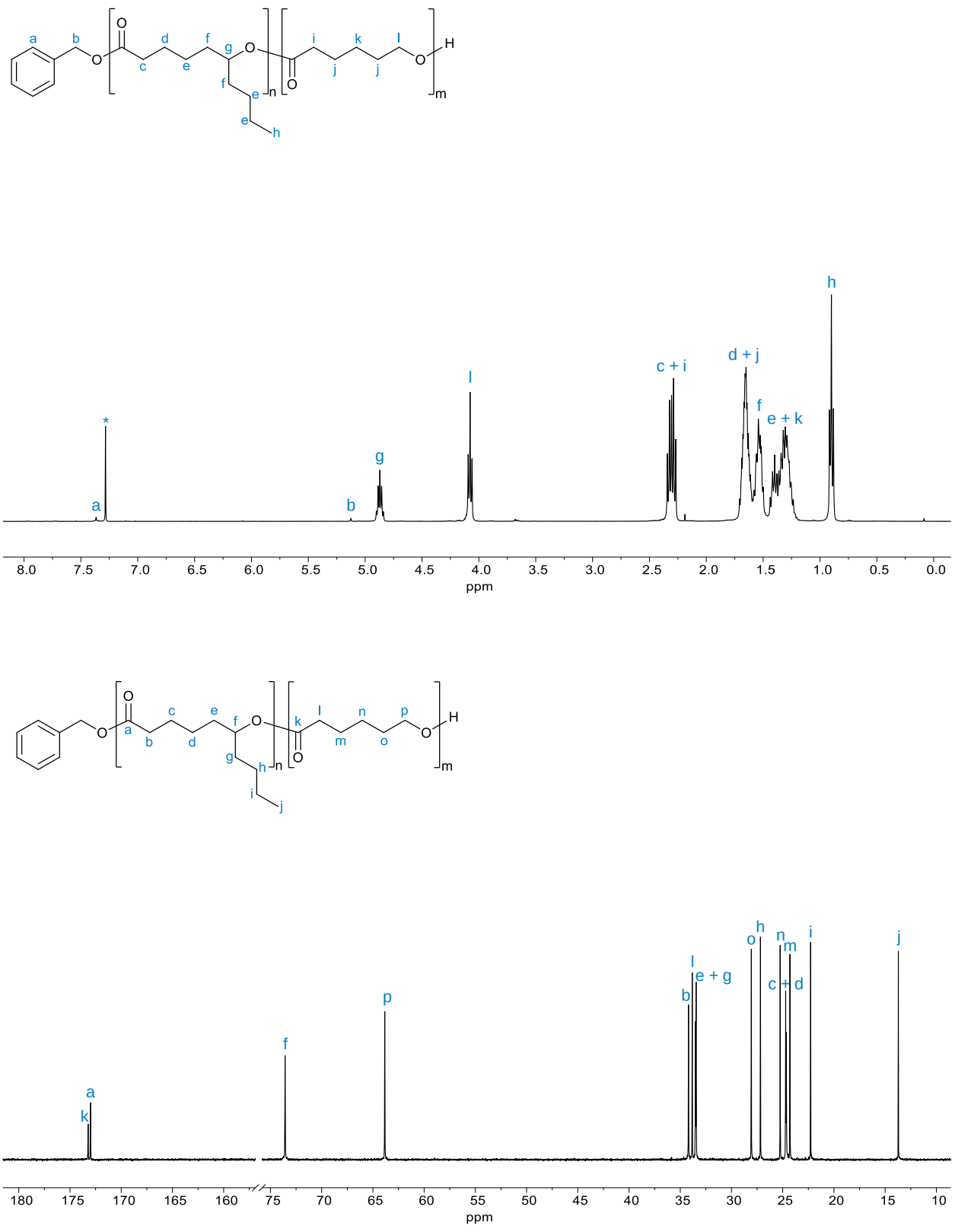

Fig. S44 ^{1}H and $^{13}C\{H\}$ NMR spectrum of poly(DL-*b*-CL) in $CDCl_3$ at 298 K.

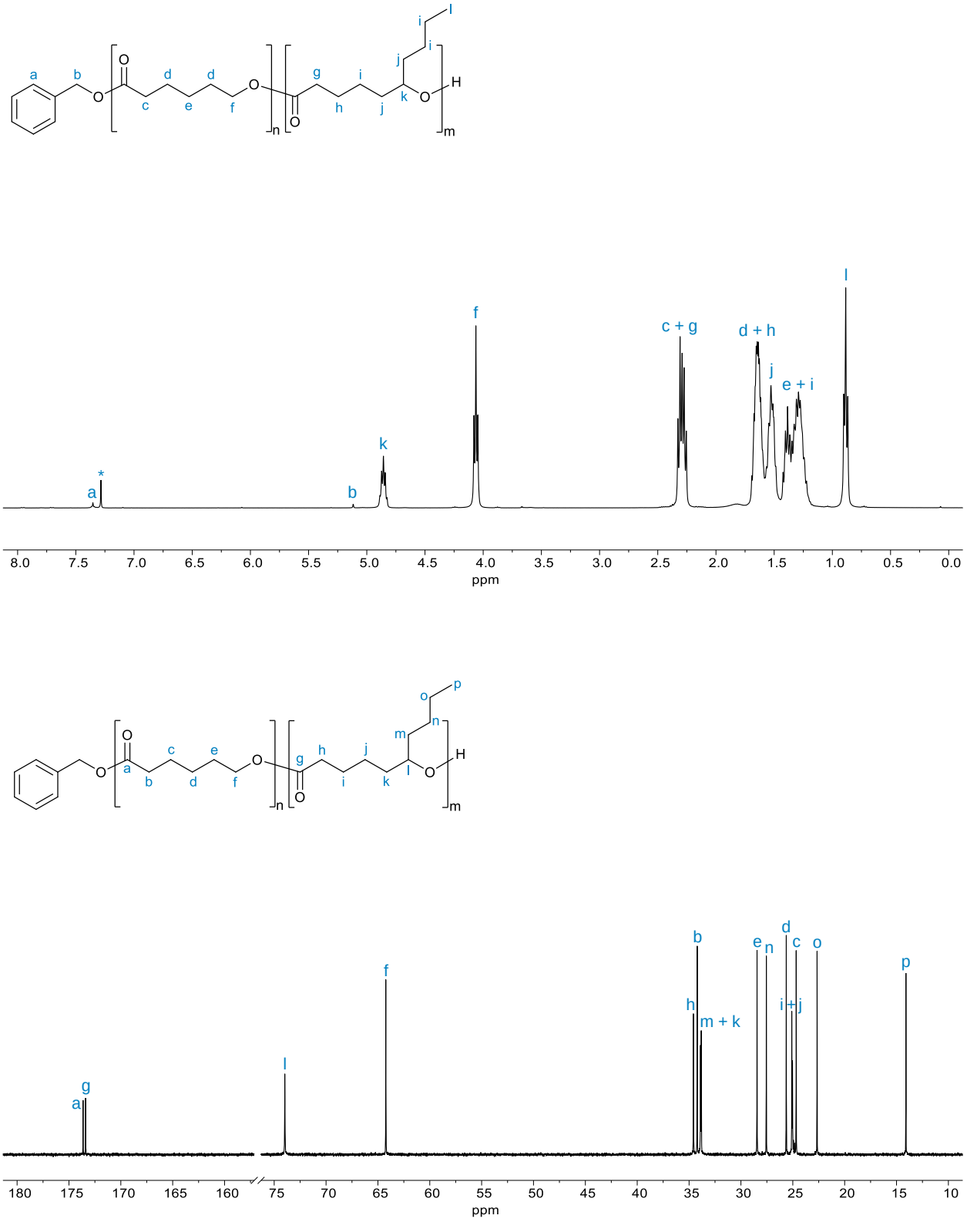

Fig. S45 ^{1}H and $^{13}C\{H\}$ NMR spectrum of poly(CL-*b*-DL) in $CDCl_3$ at 298 K.

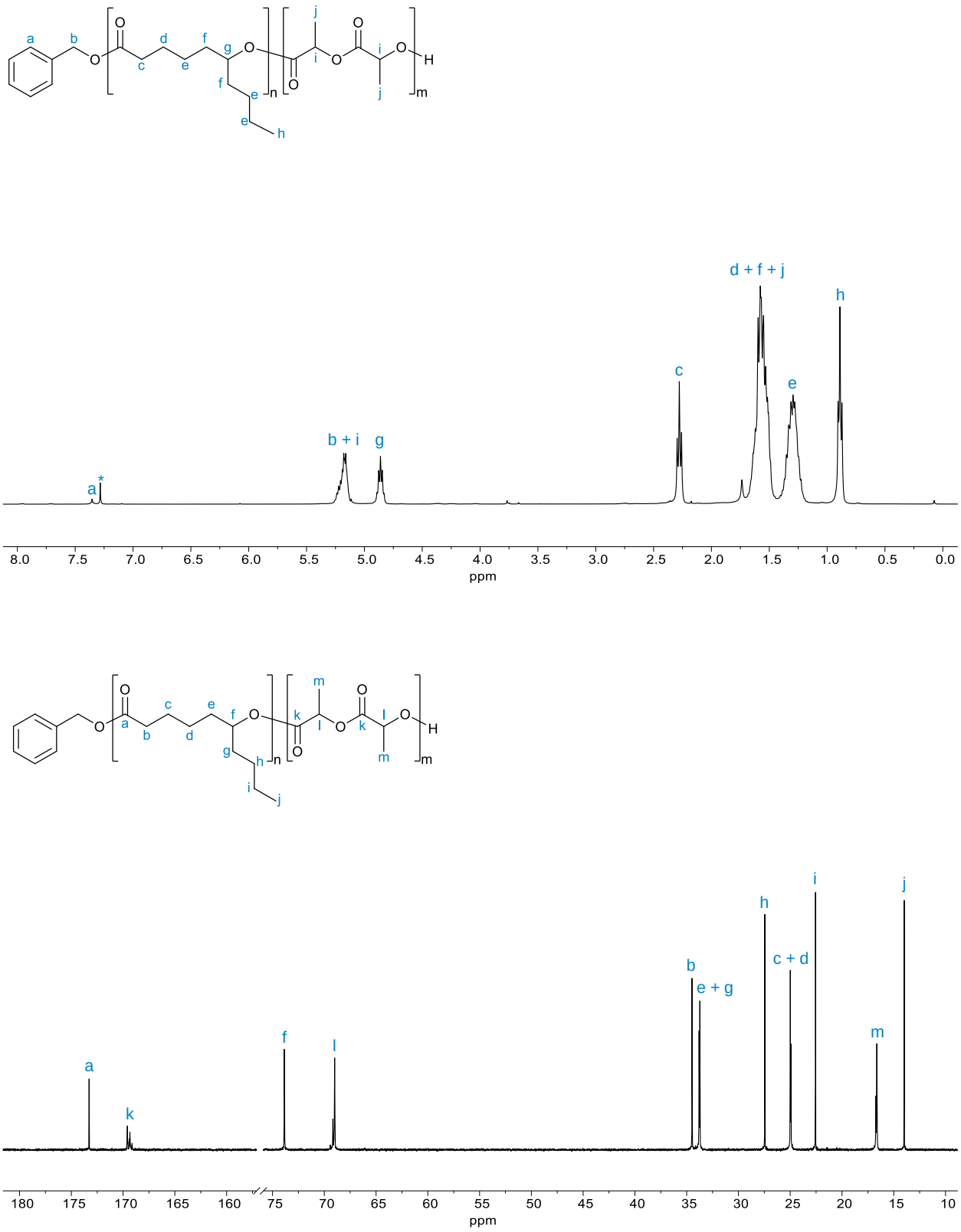

Fig. S46 ^{1}H and $^{13}C\{H\}$ NMR spectrum of poly(DL-*b*- *rac*-LA) in $CDCl_3$ at 298 K.

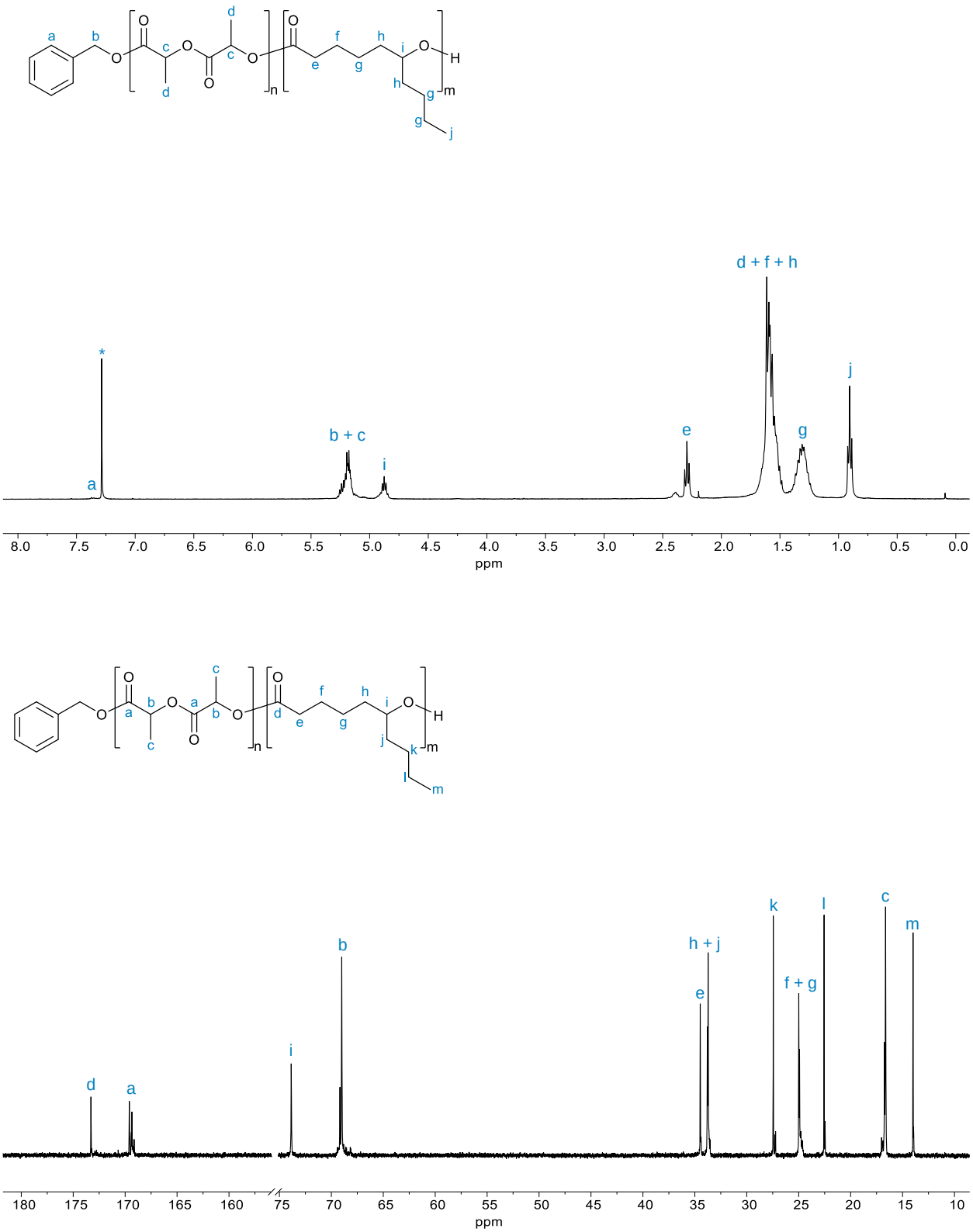

Fig. S47 ^{1}H and ^{13}C{H} NMR spectrum of poly(*rac*-LA-*b*-DL) in $CDCl_3$ at 298 K.

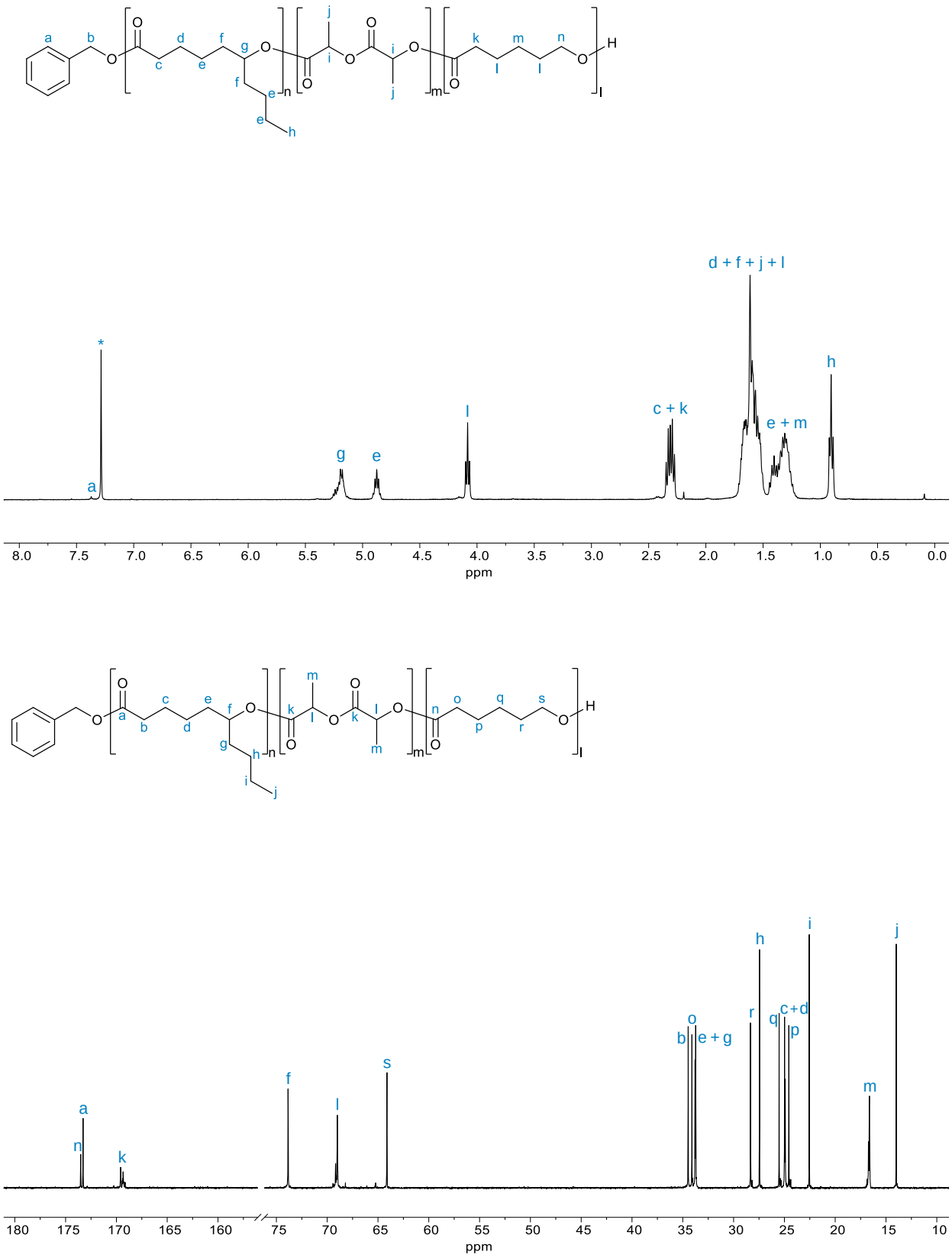

Fig. S48 ^{1}H and $^{13}C\{H\}$ NMR spectrum of poly(DL-*b*-*rac*-LA-*b*-CL) in $CDCl_3$ at 298 K.

Table S1 Copolymerization results of *rac*-LA-*r*-CL and *L*-LA-*r*-CL using complex **3** at low monomer conversion.

Entry	Monomer		Feed ratio M1:M2	Concentration (M) M1 (f_1), M2 (f_2)	Conversion (%) M1, M2	M1 (F_1), M2 (F_2) in copolymer
	M1	M2				
1	*rac*-LA	ε-CL	10:90	0.10, 0.90	7.4, 7.1	0.10, 0.90
2	*rac*-LA	ε-CL	30:70	0.30, 0.70	9.9, 11.0	0.28, 0.72
3	*rac*-LA	ε-CL	50:50	0.50, 0.50	13.0, 13.1	0.50, 0.50
4	*rac*-LA	ε-CL	70:30	0.70, 0.30	10.7, 10.9	0.70, 0.30
5	*rac*-LA	ε-CL	90:10	0.90, 0.10	9.1, 10.0	0.89, 0.11
6	*L*-LA	ε-CL	10:90	0.10, 0.90	9.9, 9.6	0.10, 0.90
7	*L*-LA	ε-CL	30:70	0.30, 0.70	8.3, 7.2	0.33, 0.67
8	*L*-LA	ε-CL	50:50	0.50, 0.50	9.1, 8.4	0.52, 0.48
9	*L*-LA	ε-CL	70:30	0.70, 0.30	9.1, 8.9	0.70, 0.30
10	*L*-LA	ε-CL	90:10	0.90, 0.10	9.9, 9.1	0.91, 0.09

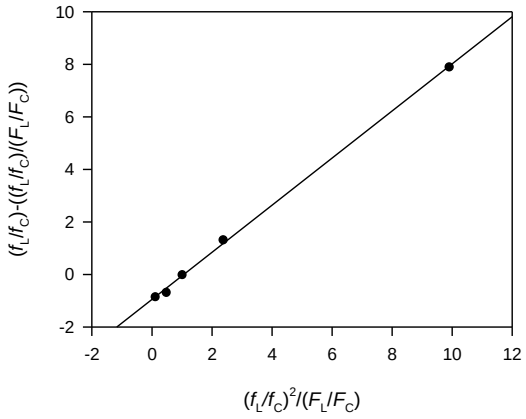

Fig. S49 Reactivity ratio of *rac*-LA and ε-CL using the Fineman–Ross method.

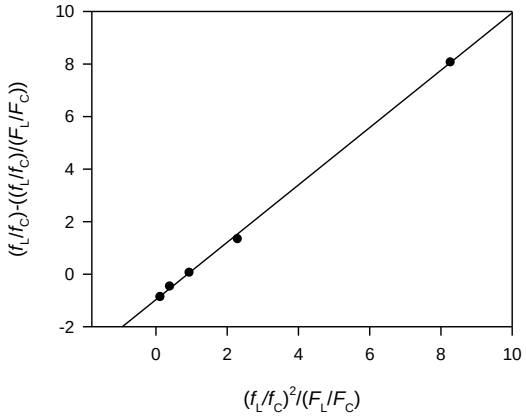

Fig. S50 Reactivity ratio of *L*-LA and ε-CL using the Fineman–Ross method.